High-Resolution Imaging of Cold Atoms through a Multimode Fiber

Nicolas Vitrant, Sébastien Garcia, Kilian Müller,[†] and Alexei Ourjoumtsev[*]
JEIP, USR 3573 CNRS, Collège de France, PSL University, 11 Place Marcelin Berthelot, 75231 Paris Cedex 05, France

(Received 18 December 2020; revised 29 April 2021; accepted 2 June 2021; published 17 June 2021)

We develop an ultracompact high-resolution imaging system for cold atoms. Its only in-vacuum element is a multimode optical fiber with a diameter of 230 μm, which simultaneously collects light and guides it out of the vacuum chamber. External adaptive optics allow us to image cold Rb atoms with approximately 1-μm resolution over a 100×100 μm^2 field of view. These optics can be easily rearranged to switch between fast absorption imaging and high-sensitivity fluorescence imaging. This system is particularly suited for hybrid quantum-engineering platforms where cold atoms are combined with optical cavities, superconducting circuits, or optomechanical devices restricting optical access.

DOI: 10.1103/PhysRevApplied.15.064047

I. INTRODUCTION

Cold atoms are powerful resources for quantum engineering. Controlling them quickly and precisely requires high-resolution optics compatible with an ultrahigh-vacuum (UHV) environment. The development of optical systems designed to manipulate single atoms [1,2] and of "quantum-gas microscopes" capable of resolving individual atoms trapped in optical lattices [3,4] has led to major breakthroughs, in particular for quantum simulations. Things become more difficult in hybrid setups, combining atoms with optical cavities, superconducting circuits, or nanostructures, where mechanical constrains prevent the use of bulk high-resolution optics. Imaging cold atoms with high resolution and guiding the light out of the vacuum system are two seemingly simple tasks that, in practice, limit the performance of many experiments.

Optical fibers intuitively seem to be a good solution for both problems at once. Single-mode fibers (SMFs) have indeed been used to trap cold atoms in predetermined configurations [5,6] but, by definition, they cannot transmit a multimode image. Multimode fibers (MMFs) were traditionally disregarded as they tend to completely randomize the transmitted wave fronts. A paradigm shift occurred with the recent development of adaptive optics. Even though a sufficiently long multimode fiber is indeed a random optical medium, it is a linear one. The transmission matrix relating the light fields in a set of input and output modes can be measured [7]. Its inverse transforms numerically randomly looking images registered at the "proximal" end of the fiber into meaningful images of an object located near the "distal" end. Alternatively, the wave fronts emerging from the fiber can be optically reshaped with use of spatial light modulators (SLMs).

In this paper, we extend these two methods, which were initially developed in the context of biological imaging [8], to the imaging of cold atoms. We use a highly multimode optical fiber acting both as a collection optic and a waveguide to image ^{87}Rb atoms optically trapped near its distal end. The fiber's total diameter of 230 μm is small enough for it to be used in many spatially constrained setups. Its high numerical aperture allows us to reach a resolution of 1.2 μm in a 100×100 μm^2 field of view. We start by describing the experimental apparatus and the way we measure the fiber's transmission matrix. We then present our results on absorption imaging of atomic clouds by digital inversion of the transmission matrix. The shadow cast by the atoms on a coherent beam injected into the fiber is reconstructed from the speckle patterns of the emerging light. We also introduce an alternative, scanning-point technique that allows both absorption imaging and incoherent fluorescence detection of small atomic samples. The light emitted from a point at the distal end of the fiber is refocused at the proximal end by a spatial light modulator, thus performing an optical inversion.

II. SETUP AND CHARACTERIZATION

In the experimental setup, we use a 25-cm-long step-index MMF with a core diameter of 200 μm and a numerical aperture of 0.5 (Thorlabs FP200ERT) as a compact optical bridge between the inside and the outside of an UHV chamber (see Fig. 1). Inside a glass cell of the UHV chamber, we create a cloud of cold ^{87}Rb atoms loaded from background vapor in a magneto-optical trap located 3 mm

[*]alexei.ourjoumtsev@college-de-france.fr
[†]Present address: LightOn, 5 Impasse Reille, Paris 75014, France

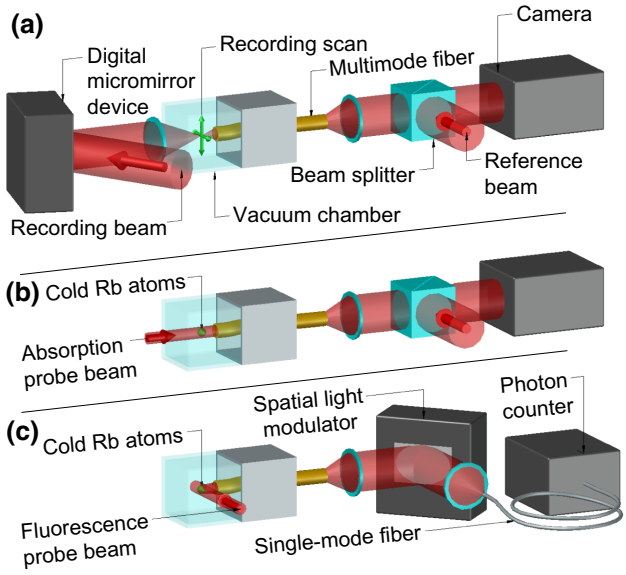

FIG. 1. Experimental setup used for imaging of cold atoms through a multimode fiber in different configurations. (a) Characterization of the transmission matrix of the fiber: we change the input mode with a DMD while interferometrically recording the output field with a camera. (b) Absorption imaging by digital inversion: we use the inverted transmission matrix to see the shadow of the atoms on a laser coupled into the fiber. (c) Fluorescence detection by optical inversion: we couple the atom emission mode to a photon counter with a SLM.

from the in-vacuum end of the MMF, referred to as the distal end in the vocabulary of endoscopy. As described in Ref. [9], we use an 800-nm laser to transport cold atoms to 200 μm from the MMF distal end and to store them there in a microtrap. This dipole-trapping laser is shaped by digital optical phase conjugation (DOPC) and sent through the MMF from its outside-vacuum end, referred to as the proximal end. On this side, a dichroic mirror allows us to separate the 800-nm-wavelength light from that of the 780-nm-wavelength atomic transition. The latter is directed to either of the two detection systems: digital-inversion imaging and optical-inversion detection, as shown in Figs. 1(b) and 1(c), respectively.

For the initial characterization of the fiber [see Fig. 1(a)], we use a digital micromirror device (DMD; Texas Instrument DLP4500NIR) to excite selected input modes of the fiber from its distal side through the vacuum glass cell. The DMD is illuminated with a collimated Gaussian laser beam, the reflection of which is then expanded by a telescope (magnification $M = 3$, not shown) and focused in the distal plane by a high-numerical-aperture aspheric condenser lens (focal length $f = 26$ mm). Thus, in contrast to usual DMD systems relying on direct imaging with binary intensity modulation, we program binary holograms on the DMD in the Fourier plane to create arbitrary light patterns in the distal plane. The binary holograms are defined by our switching on a pixel at position $\vec{r}$ on the DMD if $\cos\phi(\vec{r}) \geq 0$ [10,11], where $\phi(\vec{r})$ is the desired phase profile after the reflection. We spatially control the first order generated by a grating-patterned hologram with period $L_1 = 40$ μm (approximately eight pixels) along the horizontal axis with unit vector $\vec{e}_x$. With the corresponding linear phase $\phi(\vec{r}) = \vec{r}\cdot\vec{K}_1$, with $\vec{K}_1 = \vec{e}_x 2\pi/L_1$, the field in the distal plane is the series of focused beams of the different orders generated by the grating pattern with spacing $\lambda f/L_1 M \simeq 170$ μm for atomic resonant wavelength $\lambda \simeq 780$ nm. Because this spacing is larger than the 100-μm fiber radius, only the first order couples in the fiber at its center. From this point, we can displace this focused beam over a distance $\vec{q}$ in the distal plane by adding a linear phase $\vec{r}\cdot\vec{q}2\pi M/\lambda f$.

The holographic configuration offers three main advantages over direct imaging. Firstly, the resolution of the position $\vec{q}$ of the beam is very precise, measured to be on the order of 10 nm, because it results from the grating definition over the full DMD width. Secondly, the optical aberrations of the system can be measured and corrected efficiently [11]. To do so, we split the DMD into square zones withe sides of 19 pixels and we apply the base linear-grating pattern only in a reference zone (center) and a measured zone. In the focal plane, we observe the resulting interference fringes whose phase at the origin ($\vec{q} = 0$) corresponds to the wave-front distortion of the measured zone. As the aberrations vary with the beam's optical path, we perform this characterization for nine positions $\vec{q}_i$ roughly spanning the 100×100 μm^2 field of view, and then interpolate the wave-front corrections for arbitrary positions $\vec{q}$. Despite the use of common lenses with aberrations and defects in DMD flatness, we thus achieve a Gaussian beam waist of less than 1.2 μm over the imaging region. We perform this calibration on a separate setup, replacing the vacuum cell with a window made of the same glass with the same 2.5-mm thickness and measuring the focused field with a microscope objective (Nikon N40X-PF, numerical aperture 0.75). After installing the calibrated system in the setup, we verify that the pressure-induced bending of the vacuum cell does not modify the measured waist by scanning the position of the beam across the sharp edge between the core and the cladding of the multimode fiber and measuring the total transmitted intensity. Thirdly, arbitrary arrays of multiple focused spots at different positions are easily created by addition of their respective holograms on the DMD, without observable interferences for spot-center distances greater than 1.5 μm. We can also increase the diffraction-limited spot size by reducing the active area of the DMD, and displace the focal plane along the optical axis by adding a parabolic phase term (proportional to $||\vec{r}||^2$). We use these features of the DMD to generate microtraps for atoms by DOPC [9] and to characterize the fiber's transmission for imaging.

III. DIGITAL-INVERSION IMAGING

As a first imaging method, we use a measurement of the optical field in the proximal space to reconstruct the field in the distal space via digital inversion of the fiber's transmission matrix [7]. We define and measure the transmission matrix T on the basis of 10^4 input modes $\{\vec{d}_i\}$ of 1.2-μm waist created by the DMD setup. These modes are arranged in a planar square lattice of 100×100 spots with 1-μm spacing at 200 μm from the fiber's end face. The corresponding output modes $T\vec{d}_i$ are measured by off-axis holography [12], where we combine on a beam splitter the output field and a coherent reference beam with a small angle α between their propagation axes. Thus, the measured light intensity on the camera (Hamamatsu ImagEM X2 C9100-23B) exhibits interference fringes with period $|\lambda/\sin\alpha|$ (see Fig. 2). Taking digitally the Fourier transform of this image, we observe separated orders corresponding to multiples of the wavevector associated with the fringes. We isolate the first order and perform an inverse Fourier transform to recover the complex output field. For diffraction orders to be separated in Fourier space, the minimum speckle grain size l_{spc} must satisfy $l_{\mathrm{spc}} \geq 8l_{\mathrm{pxl}}$, with l_{pxl} the pixel size of the camera. The magnification of the output field and the angle of the reference beam are optimized to reach this limit, which forces the signal to be spread over many pixels. Nevertheless, off-axis holography allows us to measure a complex field with a single image. This feature has particular importance in cold-atom setups, where imaging is almost always a destructive operation and where atomic cloud preparation usually requires several seconds. For the output basis $\{\vec{p}_i\}$ of the proximal space that completes the definition of the fiber's transmission matrix, we select the 10^4 pixels of the measured field that have the highest amplitude average over the input modes, offering the strongest signal. This square $10^4 \times 10^4$ transmission matrix T is an empirical compromise between imaging quality and the computer resources needed to store and invert images on the fly. If the imaged object is localized in a smaller field of view, the number of input modes can, of course, be reduced. The number of output modes should exceed the number of modes effectively excited in the fiber to avoid reduction of the optical resolution, which is limited in our case by the 1.2-μm waist of the probe. We measure T every week, a time span over which we observe only marginal degradation of the imaging quality (see the Appendix). As experimental errors on small eigenvalues of T have a large effect on T^{-1}, we use the mean square optimized inverting operator $W = (T^\dagger \cdot T + \sigma I)^{-1} \cdot T^\dagger$, with σ the standard deviation of the experimental noise and I the identity matrix [13]. Thus, from a measured field $\vec{p}$ in the proximal space, we get an image $W\vec{p}$ of the field in the distal space. This technique corrects for the aberrations of all optical elements located between the in-vacuum object plane and the beam splitter, where the probe and reference beams interfere. This, of course, includes the multimode fiber, but also the collimation lens collecting light at its proximal end. Therefore, as long as its numerical aperture exceeds that of the fiber, the optical quality of this lens is unimportant, allowing us to use a cheap aspheric condenser (Thorlabs ACL12708U-B).

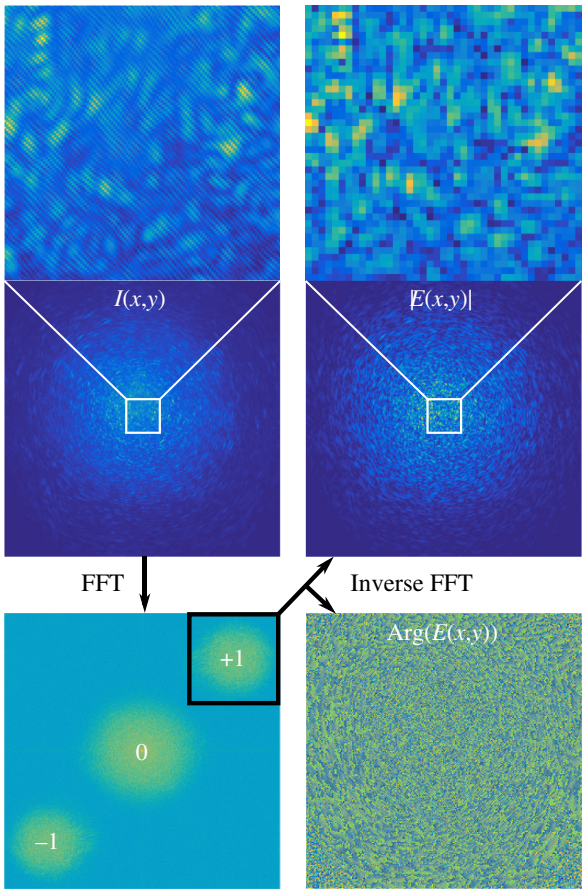

FIG. 2. Reconstruction of the proximal speckle field by off-axis holography [12]. The collimated speckle emerging from the fiber interferes with a reference beam. A small angle between their propagation axes leads to interference fringes on the measured intensity $I(x,y)$ (upper-left panel, central area enlarged). Because of this modulation, the Fourier transform of this image (bottom-left panel) exhibits diffractionlike localized orders. Selecting the order $+1$ allows one to isolate the interference term and, by inverse Fourier transform, to recover the amplitude (upper-right panel, central area enlarged) and the phase (lower-right panel) of the complex speckle field.

We apply this digital-inversion technique to image cold atoms by absorption. While the reconstructed field intensity $I_{(a)}$ of a laser beam sent into the fiber has a Gaussian profile [Fig. 3(a)], a cold atomic cloud in a 1.2-μm-waist microtrap casts a shadow at its center [Fig. 3(b)]. The corresponding optical depth [equal to $\ln\left(I_{(a)}/I_{(b)}\right)$ where $I_{(a)}$ and $I_{(b)}$ are, respectively, the intensities measured without and with the atoms], shown in Fig. 3(c), is proportional to

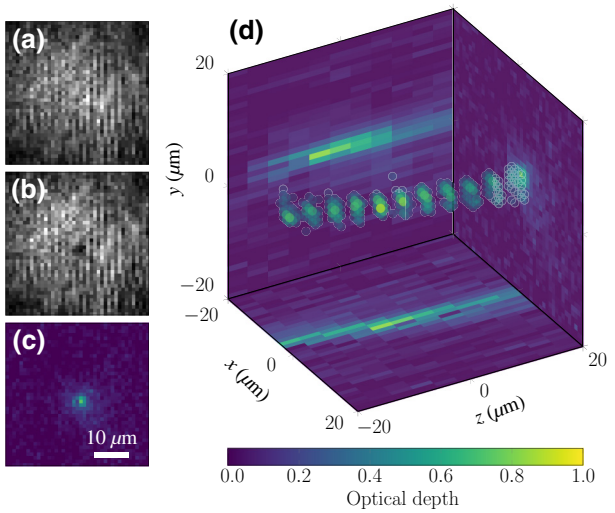

FIG. 3. Absorption imaging through the multimode fiber by digital inversion. (a),(b) Light intensity in the distal plane, (a) without and (b) with atoms (100 averages). (c) Optical depth of the atomic cloud, proportional to the atomic density integrated along the detected mode, extracted from (a),(b). (d) Optical depth reconstructed by digital inversion toward multiple distal planes separated by 4 μm. Sides of the three-dimensional box show cuts through the point of maximum optical depth.

the atomic density of the cloud. The observed sharp peak, with a Gaussian rms radius of 1.7 μm, demonstrates the high resolution of digital-inversion imaging of cold atoms through the multimode fiber. We use this imaging to make temperature measurements with the time-of-flight method or to determine the atomic distribution in multiple trap geometries [9].

This holographic measurement of the field provides two additional advantages. Firstly, one could use it for phase-contrast imaging, a powerful method to characterize very dense atomic clouds such as Bose-Einstein condensates [14]. Secondly, the field can be reconstructed for several distal planes from a single measurement by use of the corresponding inverting matrices, allowing numerical refocusing. As shown in Fig. 3(d), by numerically scanning the position of the distal object plane and measuring the corresponding variations of the integrated absorption, we can reconstruct the axial length of our atomic cloud determined by the Rayleigh length of the trapping beam, convoluted with the 6-μm depth of focus defined by the Rayleigh range of the Gaussian detected mode.

IV. OPTICAL-INVERSION DETECTION

The digital-inversion technique is a powerful method for absorption imaging of dense atomic clouds; however, it has two main limitations. Firstly, the interferometric imaging of the speckle field emerging from the multimode fiber requires the signal to be spread over the full camera sensor, even when the imaged object is very localized: in this case, traditional imaging would project it on a few camera pixels and offer a greater signal-to-noise ratio. Secondly, the measurement relies on a coherent probe field and thus it cannot detect the fluorescence photons emitted by atoms with random phases.

To overcome these limitations, we introduce another detection method: by optical inversion on a SLM, we send light coming from a chosen point in the object plane to a photon counter (a highly efficient single-pixel detector) via a SMF; see Fig. 1(c). We use DOPC with a setup similar to the one used to transport and trap the atoms [9]. During the characterization, for each pixel mode generated by the DMD in the distal plane, we measure the interference pattern between the speckle emerging at the proximal side and a reference beam from the SMF. By using three-image phase-shifting interferometry, we determine the spatial phase pattern of the speckle relative to the SMF beam. To detect efficiently the photons emitted in the corresponding input mode, we apply the conjugate phase pattern on the SLM, which then couples the MMF output mode into the SMF input. We then connect the SMF output to a silicon avalanche photodiode in photon-counting mode (Excelitas SPCM-NIR-24). The role of the SMF is to enhance the detector's spatial-mode selectivity and to simplify its isolation from ambient light. The photon counter could be replaced by a single pixel of a camera or by a photomultiplier; our choice is guided by its comparatively high efficiency, low noise, and high bandwidth. In addition to its ability to image incoherent light, for dim localized sources this technique offers a greater signal-to-noise ratio than digital-inversion imaging, as the noise of many pixels required to measure a speckle is replaced with the noise of just pixel. The price to pay is the need to scan the imaged spot in the distal plane instead of getting a full-field image in one shot, leading to a slower measurement rate. The resolutions of both approaches are measured to be similar: the setup for optical inversion is identical to the one we use to generate optical microtraps through the multimode fiber, where light propagates in the opposite direction and can be focused down to 1.2-μm spots near the atoms [9].

As a first application, we use this optical-inversion detection to measure the absorption of atoms in a microtrap. We change sequentially the SLM phase pattern to displace the detected mode in the distal plane with 0.5-μm spacing. The resulting image of optical density, presented in Fig. 4(a), shows a sharp peak corresponding to the center of the dipole trap, thus demonstrating high resolution. This optical-inversion detection requires the measurement to be repeated to build an image by scanning pixel by pixel. However, the noise per pixel is here significantly lower, with a standard deviation of 0.049(3) for five averages, than in digital-inversion imaging, which requires 100 averages to reach a similar standard deviation of 0.032(3).

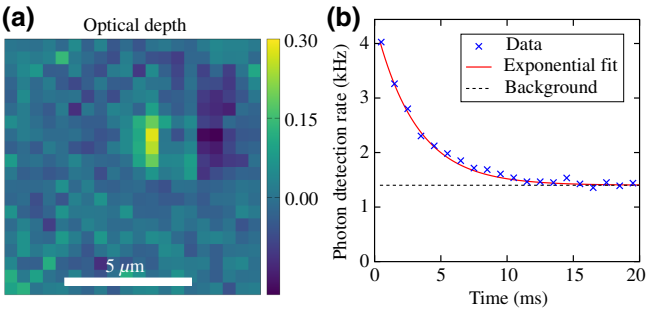

FIG. 4. Detection through the multimode fiber by optical inversion. (a) Absorption observed pixel by pixel on the photon counter while we displace the detected mode of the input plane with the SLM (averaged over five repetitions per pixel). (b) Detected fluorescence on the photon counter as function of time after atom illumination starts (averaged over 10^4 repetitions).

As a second application, we observe the incoherent fluorescence of atoms. We select the detection mode corresponding to the trap's center, where we observe the highest absorption. We illuminate the atoms with a resonant laser beam orthogonal to the fiber's axis, with a 50-μm Gaussian waist and an intensity nearly saturating the atomic transition [see Fig. 1(c)]. In Fig. 4(b), the detected photon rate decays exponentially with a time constant of 3.1-ms. This represents the atom lifetime in the trap, dominated by heating from repeated absorption and emission of photons. The 1.4-kHz background level stems from the spurious coupling to fiber modes of photons from the illuminating beam (1.1 kHz), the anti-Stokes Raman backscattering [15] in the MMF from the trapping light (0.2 kHz), and the dark counts of the detector (0.1 kHz). The level of Raman backscattering is considerably reduced in comparison with that in atom microtraps based on a single-mode fiber [6] because of a marginal overlap of trapping light and detection light in the fiber. The initial 2.6-kHz detected photon rate above the background indicates the presence of approximately three atoms on average in the microtrap before the illumination starts.

We deduce this atom number from the estimated total fluorescence detection efficiency $\eta_{\mathrm{tot}} \simeq 8 \times 10^{-5}$, which results from different contributions as $\eta_{\mathrm{tot}} = \eta_{\mathrm{col}}\eta_{\mathrm{SLM}}\eta_{\mathrm{opt}}\eta_{\mathrm{PC}}$. While the losses on standard optical elements ($\eta_{\mathrm{opt}} \simeq 0.9$, in particular on optical filters) and the photon-counter efficiency ($\eta_{\mathrm{PC}} \simeq 0.7$) are not negligible, the dominant contributions are the collection efficiency ($\eta_{\mathrm{col}} \simeq 1.3\%$) and the SLM efficiency ($\eta_{\mathrm{SLM}} \simeq 1\%$). The collection efficiency is the calculated overlap between the spherical spontaneous-emission mode of the atom and the 1.2-μm-waist Gaussian detected mode. It has the same order of magnitude as the efficiencies obtained for atomic microtraps with aspheric lenses [6,16]. The SLM efficiency is an important limiting factor in our detection, but it also has a huge potential for improvements. First, the SLM used (Hamamastu X10468-03) has absorption losses of 50% at 780 nm, and these losses can be reduced to a few percent with other commercial models. Second, our system corrects only for a single polarization component of the speckle (approximately 40% losses) and full polarization control could be achieved by use of two SLMs or two SLM sides [17]. The third and most-important contribution is the approximately 4% diffraction efficiency of the wave-front correction. Limited by our SLM resolution (792×600), this diffraction efficiency could be increased significantly toward the $\pi/4 \simeq 79\%$ limit of phase modulation [18] with a higher-resolution SLM (4160×2464 available). Such improvements would bring the detection method to the regime of single-atom single-shot detection. We are currently at the edge of this regime with a signal of approximately two detected photons per emitting atom for four photons of noise during the 3.1-ms lifetime. They would also enable the real-time imaging of single-atom arrays, either sequentially by scanning the detected mode over the positions of the atomic traps or simultaneously by conjugating each trap with a different detector or pixel of an electron-multiplying-CCD camera using multiple-plane light conversion to preserve the overall efficiency [19].

V. CONCLUSION

The results presented here are from an attempt to use a multimode fiber to image cold atoms. Compared with traditional optical systems based on bulk aspheric lenses, it offers additional features such as the absence of a fixed working distance and a compactness that could be a game-changer for many experiments. Many of its drawbacks could be easily dealt with in future experiments using modern hardware and eliminating initial mistakes. In particular, the fiber's transmission matrix can be easily made much stabler by eliminating or relocating the atomic dispensers, which are currently placed only a few millimeters from the fiber and heated above 500 °. Depending on the experimental requirements, a gradient-index fiber with a slightly lower numerical aperture could also offer greater stability [20]. Alternatively, one could use a shorter fiber, allowing *a priori* modeling [21], or imprint a partially reflective pattern on its distal end to act as a permanently fixed calibration reference [22]. Thus, we realistically expect that the need to optically access the distal end of the fiber for periodic recalibrations can be eliminated, making this optical system a viable and advantageous alternative to traditional ones by allowing compact imaging of cold-atom clouds or single-shot detection of single atoms.

ACKNOWLEDGMENTS

This work was funded by the DIM SIRTEQ project LECTRA, IDEX Grant No. ANR-10-IDEX-001-02-PSL

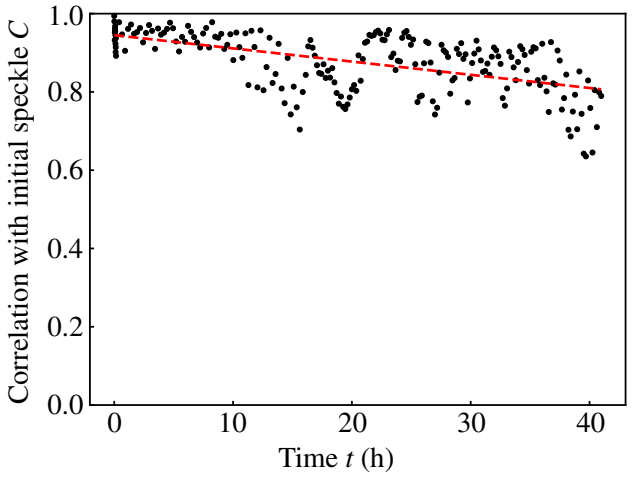

FIG. 5. Correlation coefficient C between the measured speckle image at time t and the initial speckle image at $t = 0$. The dashed red line is the linear function that fits best to the black data points.

PISE, and European Research Council Starting Grant SEAQUEL. A.O. is a CIFAR Azrieli Global Scholar. The authors thank P. Travers and F. Moron for technical support, Q. Lavigne, T. Kouadou, and J. Vaneecloo for their assistance at the early stage of the project, and S. Gigan for fruitful discussions.

APPENDIX: LONG-TERM STABILITY OF FIBER TRANSMISSION

The transmission matrix of the fiber changes on a long-term timescale. To characterize this effect, we measure over time the output speckle intensity resulting from a 1.2-μm focused laser beam in the distal plane. Each image I_t acquired at time t is compared with the initial speckle image I_0 recorded at time $t = 0$ by our calculating the correlation coefficient $C = \langle (I_t - \langle I_t \rangle) \times (I_0 - \langle I_0 \rangle) \rangle / \sqrt{\langle (I_t - \langle I_t \rangle)^2 \rangle \langle (I_0 - \langle I_0 \rangle)^2 \rangle}$, where the average $\langle \cdot \rangle$ is taken over the pixels and the $\times$ product is taken pixelwise. In Fig. 5, we observe a long-term decay of the correlation coefficient C. The linear fit of the data (by the function $C_0 - t/t_s$) provides a lower limit of $t_s \simeq 12$ days for the characteristic stability time of the fiber's transmission matrix. Operations relying on this matrix, such as atomic manipulation and imaging, are efficient as long as a significant amount of correlation remains. Thus, the stability of the transmission matrix allows us to use a single characterization over the 5 days of a workweek.

[1] N. Schlosser, G. Reymond, I. Protsenko, and P. Grangier, Sub-poissonian loading of single atoms in a microscopic dipole trap, Nature **411**, 1024 (2001).

[2] D. Barredo, V. Lienhard, S. de Léséleuc, t. Lahaye, and A. Browaeys, Synthetic three-dimensional atomic structures assembled atom by atom, Nature **561**, 79 (2018).

[3] W. S. Bakr, J. I. Gillen, A. Peng, S. Fölling, and M. Greiner, A quantum gas microscope for detecting single atoms in a Hubbard-regime optical lattice, Nature **462**, 74 (2009).

[4] J. F. Sherson, C. Weitenberg, M. Endres, M. Cheneau, I. Bloch, and S. Kuhr, Single-atom-resolved fluorescence imaging of an atomic Mott insulator, Nature **467**, 68 (2010).

[5] E. Vetsch, D. Reitz, G. Sagué, R. Schmidt, S. T. Dawkins, and A. Rauschenbeutel, Optical Interface Created by Laser-Cooled Atoms Trapped in the Evanescent Field Surrounding an Optical Nanofiber, Phys. Rev. Lett. **104**, 203603 (2010).

[6] S. Garcia, D. Maxein, L. Hohmann, J. Reichel, and R. Long, Fiber-pigtailed optical tweezer for single-atom trapping and single-photon generation, Appl. Phys. Lett. **103**, 114103 (2013).

[7] S. M. Popoff, G. Lerosey, R. Carminati, M. Fink, A. C. Boccara, and S. Gigan, Measuring the Transmission Matrix in Optics: An Approach to the Study and Control of Light Propagation in Disordered Media, Phys. Rev. Lett. **104**, 100601 (2010).

[8] I. N. Papadopoulos, S. Farahi, C. Moser, and D. Psaltis, High-resolution, lensless endoscope based on digital scanning through a multimode optical fiber, Biomed. Opt. Express **4**, 260 (2013).

[9] N. Vitrant, K. Müller, S. Garcia, and A. Ourjoumtsev, Manipulating cold atoms through a high-resolution compact system based on a multimode fiber, Opt. Lett. **45**, 1519 (2020).

[10] W.-H. Lee, Binary computer-generated holograms, Appl. Opt. **18**, 3661 (1979).

[11] P. Zupancic, P. M. Preiss, R. Ma, A. Lukin, M. E. Tai, M. Rispoli, R. Islam, and M. Greiner, Ultra-precise holographic beam shaping for microscopic quantum control, Opt. Express **24**, 13881 (2016).

[12] E. Cuche, F. Bevilacqua, and C. Depeursinge, Digital holography for quantitative phase-contrast imaging, Opt. Lett. **24**, 291 (1999).

[13] S. Popoff, G. Lerosey, M. Fink, A. C. Boccara, and S. Gigan, Image transmission through an opaque material, Nat. Commun. **1**, 1 (2010).

[14] C. C. Bradley, C. A. Sackett, and R. G. Hulet, Bose-Einstein Condensation of Lithium: Observation of Limited Condensate Number, Phys. Rev. Lett. **78**, 985 (1997).

[15] M. A. Farahani and T. Gogolla, Spontaneous raman scattering in optical fibers with modulated probe light for distributed temperature raman remote sensing, J. Lightwave Technol. **17**, 1379 (1999).

[16] Y. R. P. Sortais, H. Marion, C. Tuchendler, A. M. Lance, M. Lamare, P. Fournet, C. Armellin, R. Mercier, G. Messin, A. Browaeys, and P. Grangier, Diffraction-limited optics for single-atom manipulation, Phys. Rev. A **75**, 013406 (2007).

[17] I. Moreno, J. A. Davis, T. M. Hernandez, D. M. Cottrell, and D. Sand, Complete polarization control of light from a liquid crystal spatial light modulator, Opt. Express **20**, 364 (2012).

[18] T. Čižmár and K. Dholakia, Shaping the light transmission through a multimode optical fibre: Complex transformation analysis and applications in biophotonics, Opt. Express **19**, 18871 (2011).

[19] G. Labroille, B. Denolle, P. Jian, P. Genevaux, N. Treps, and J.-F. Morizur, Efficient and mode selective spatial mode multiplexer based on multi-plane light conversion, Opt. Express **22**, 15599 (2014).

[20] A. M. Caravaca-Aguirre and R. Piestun, Single multimode fiber endoscope, Opt. Express **25**, 1656 (2017).

[21] M. Plöschner, T. Tyc, and T. Čizmár, Seeing through chaos in multimode fibres, Nat. Photonics **9**, 529 (2015).

[22] R. Y. Gu, R. N. Mahalati, and J. M. Kahn, Design of flexible multi-mode fiber endoscope, Opt. Express **23**, 26905 (2015).